Journal of *Marine Science and Engineering*

MDPI

Article

Unraveling the Evolution of a Submerged Coastal Karst Basin in the Adriatic Sea: Insights from Geomorphology and Seismic Stratigraphy

Dea Brunović, Ozren Hasan *, Nikolina Ilijanić and Slobodan Miko

Croatian Geological Survey, Sachsova 2, 10000 Zagreb, Croatia; dbrunovic@hgi-cgs.hr (D.B.); nilijanic@hgi-cgs.hr (N.I.); smiko@hgi-cgs.hr (S.M.)
* Correspondence: ohasan@hgi-cgs.hr

Abstract

Although recent studies have significantly improved our understanding of submerged landscapes along the karstified eastern Adriatic coast, many aspects of their evolution and response to post-glacial relative sea-level rise remain poorly understood. Thus, the present study offers new insights into the Late Quaternary paleoenvironmental history of Pirovac Bay, a submerged coastal karst basin in the central Adriatic, by integrating high-resolution seismic data with chronologically constrained sediment cores. The results revealed the existence of two morphologically distinct karst depressions that provided accommodation space for the formation of diverse depositional environments. The Late Glacial and Holocene sedimentary succession documents an evolution from subaerial and fluvially influenced settings to lacustrine and ultimately fully marine environmental conditions. The identified fluvio-karst valley highlights the largely unexplored role of fluvio-karst processes in the development of coastal karst basins, while the discovered Pirovac paleolake is the youngest submerged Holocene lake known along the eastern Adriatic coast. The present-day embayment appears to be characterized by erosional processes and active submarine groundwater discharge, reflecting highly dynamic hydrological conditions. These findings contribute to a better understanding of the interactions between karstification, sea-level rise, sedimentary processes, and groundwater dynamics in coastal karst basins. They also provide an important framework for future paleoenvironmental and hydrogeological investigations along the eastern Adriatic coast.

Keywords: Quaternary; submerged landscapes; fluvio-karst; paleolake; sea-level rise; submarine groundwater discharge

Check for updates

Academic Editor: Charitha Pattiaratchi

Received: 9 June 2026
Revised: 21 July 2026
Accepted: 22 July 2026
Published: 24 July 2026

Copyright: © 2026 by the authors. Licensee MDPI, Basel, Switzerland. This article is an open access article distributed under the terms and conditions of the Creative Commons Attribution (CC BY) license.

1. Introduction

The Mediterranean region is characterized by extensive karst landscapes shaped by prolonged karstification, which has produced diverse landforms, including karst lakes, karst poljes, caves, and dolines [1–4]. Many of these settings preserve valuable sedimentary records that enable the reconstruction of Quaternary paleoenvironmental variability [5–7]. Karst terrains in coastal zones were strongly influenced by Quaternary sea-level changes associated with glacial-interglacial cycles [8,9], which controlled shoreline migration and governed the dynamics between subaerial exposure and marine inundation. Following the Last Glacial Maximum (LGM), rapid sea-level rise led to the complete or partial inundation of many coastal karst areas [10–15], resulting in a major transformation of formerly terrestrial landscapes and altering their hydrology, environmental conditions, and sediment

accumulation. To date, most research has concentrated on submerged caves [14,16,17], whereas geomorphological and stratigraphic investigations of other submerged karst landforms in the Mediterranean are still relatively scarce [18,19]. Understanding these paleoenvironmental transformations and the processes that affect them is essential for deciphering how present-day Mediterranean coastal zones will evolve in response to ongoing sea-level rise [20].

One of the key characteristics of karst settings is their distinctive hydrology [4,21–25]. In coastal karst basins that encompass depression-like karst features in the coastal zone, the groundwater level is directly controlled by the sea level owing to the porous nature of such environments [26,27]. Consequently, complex hydrogeological conditions often develop, with the saline groundwater occurring below the freshwater or brackish meteoric lens. Estavelles, coastal and submarine springs are evidence of karst subsurface circulation, which act as conduits for both freshwater discharge and seawater intrusion [24,28]. These karst features may occur as submerged dolines and pockmarks, or as more diffuse seepage zones [29–31]. In addition to the subsurface groundwater network, fluvio-karst systems have an important role in the interaction between surface runoff and subsurface flow [4,28,32–35]. They may form fluvial valleys and ponors (i.e., swallow holes) that extend toward or influence the coastal and submarine environments.

Coastal karst basins are therefore transitional settings where terrestrial and marine processes converge, resulting in variable hydrological regimes and unique depositional successions that record past environmental conditions and relative sea-level changes [26]. Such settings have been documented previously in different regions worldwide, including the Yucatan [36], Bahamas [37], the Red Sea [38,39] and the Adriatic Sea [40,41]. Similar basins, albeit non-karst in origin, occur at higher altitudes and are commonly referred to as isolation basins [42,43]. Beyond the paleoenvironmental context, coastal karst basins are important for water resource management, as karst aquifers are highly vulnerable to salinization driven by sea-level rise, groundwater exploitation, and changing hydrological conditions [44].

With the overall aim of advancing the existing knowledge of coastal karst basins, we investigate a completely submerged karst basin in the present-day Pirovac Bay. While a previous multi-proxy study of sediment cores revealed that the Pirovac Bay basin functioned as a freshwater paleolake prior to Holocene marine transgression [45], its geomorphological framework and sedimentary architecture have not yet been described in detail. This study thus focuses on reconstructing the paleoenvironmental conditions that led to its submergence and on evaluating how the geomorphological setting and complex karst hydrology influenced its evolution. In particular, we aimed to investigate basin geomorphology using high-resolution seismic data and infer depositional environments by combining seismic and sediment core data. Finally, Pirovac Bay and the adjacent Lake Vrana near Biograd na Moru provide an excellent natural setting for assessing the role of groundwater and sea-level interactions and deciphering their hydrological connectivity through both surface and subsurface pathways. These results provide new insights into the functioning of submerged coastal karst basins and contribute to a better understanding of their responses to past and future sea-level changes.

2. Study Area

Pirovac Bay (43°50′ N, 15°37′ E) is located along the eastern Adriatic coast (Figure 1A), which is part of the Adriatic Carbonate Platform that formed during the Early Jurassic and eventually disintegrated during the Late Cretaceous [46]. The platform succession is predominantly composed of shallow-marine limestones and dolomites. Its fragmentation was followed by the deposition of Paleogene limestones and flysch deposits, coinciding

with the onset of karstification. This process continued throughout the Quaternary, ultimately shaping the present-day Dinaric karst landscape. As a result, various characteristic karst geomorphological features have developed, including dolines, karst poljes, river valleys, canyons, and caves [47], many of which often act as sediment traps [48,49]. Considering that a large part of the northern Adriatic shelf is very shallow, post-LGM sea-level changes had a major influence on sedimentary dynamics and regional paleoenvironmental development [40,50–53].

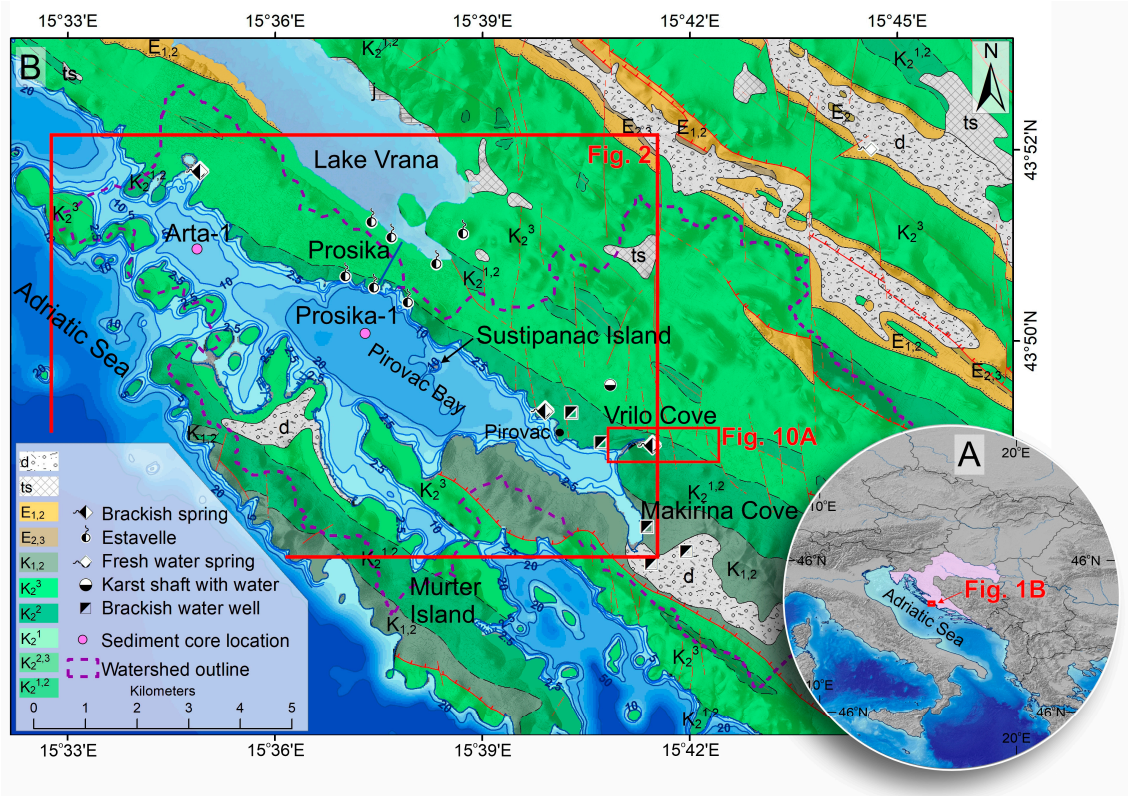


Figure 1. (**A**) Geographic location of the study area; (**B**) Geological setting of the catchment area (modified after [54,55]). The lithological units shown on the map include: $K_{1,2}$ Albian–Cenomanian dolomites; $K_2^{1,2}$ Cenomanian–Turonian limestones and dolomites; K_2^3 Early Senonian rudist limestones; $E_{1,2}$ Lower and Middle Eocene foraminiferal limestones; $E_{2,3}$ Middle Eocene flysch and conglomerates; ts Quaternary terra rossa; and d Quaternary colluvial-deluvial deposits.

Pirovac Bay is an approximately 12.5 km long and less than 3 km wide embayment, elongated in a NW-SE direction, with a surface catchment area of approximately 90.8 km^2 (Figure 1B). The bay is bounded by the mainland to the northeast and by Murter Island and numerous smaller islets to the southwest. Water depths reach up to 26 m in the central part of the bay, whereas the eastern and western sides are generally shallower than 20 m (Figure 1B). The eastern part of the bay is connected to Makirina Cove, a shallow embayment up to 2 m deep that has previously been investigated for the geochemical characterization of its organic-rich sediments [55,56] and ancient saltpans used as indicators of past sea-level change [57]. Opposite Makirina Cove is the smaller Vrilo Cove, which continues inland as an approximately 2.5 km long eastward-oriented dry valley (Figure 1B). Currently, there are no major surface freshwater flows within the catchment.

The geological setting of the Pirovac Bay catchment area is dominated by Cretaceous carbonates, primarily dolomites and limestones [54,58] (Figure 1B). The oldest lithostratigraphic unit in the area consists of Albian-Cenomanian dolomites ($K_{1,2}$), which form the core of an anticline structure oriented in the NW-SE direction. This unit extends beneath

Pirovac Bay, where it is submerged by the sea. The northern and northeastern coasts of the bay are composed of Cenomanian-Turonian limestones and dolomites ($K_2^{1,2}$). Early Senonian rudist limestones (K_2^3) are the most prevalent unit within the catchment area and around Lake Vrana near Biograd na Moru. The Cretaceous rocks are transgressively overlain by Paleogene deposits, which occur locally within the catchment area. In the surrounding area, the most prominent Paleogene deposits are Middle Eocene marl/sandstone alterations known as flysch ($E_{2,3}$), together with less common Lower and Middle Eocene foraminiferal limestones ($E_{1,2}$). Quaternary deposits comprise terra rossa and colluvial-deluvial deposits, which partially cover older units (Figure 1B).

Pirovac Bay borders Lake Vrana near Biograd na Moru, the largest freshwater lake in Croatia, characterized by a mean depth of only 2 m and a maximum depth of 4 m [45]. Lake Vrana is primarily recharged by precipitation, stream inflow, and groundwater discharge from the subaqueous springs. It is separated from the Pirovac Bay by a narrow zone of karstified limestone, ranging from 800 to 2500 m in width (Figure 1B). Despite this physical barrier, the lake and adjacent marine environment are hydrologically connected through the 800 m long Prosika artificial canal located in the southwestern part of the lake (Figure 1B). The occurrence of freshwater springs along the Pirovac Bay coast and brackish springs on the Lake Vrana side, which act as estavelles, indicates seawater intrusion into the lake system through karstified subsurface pathways along an approximately 1 km wide zone in the southeastern part of the lake (Figure 1B) [56,59–61].

3. Materials and Methods

3.1. High-Resolution Seismic Survey

A dense grid of high-resolution seismic profiles with a length of approximately 143 km was acquired throughout Pirovac Bay in June 2015 (Figure 2).

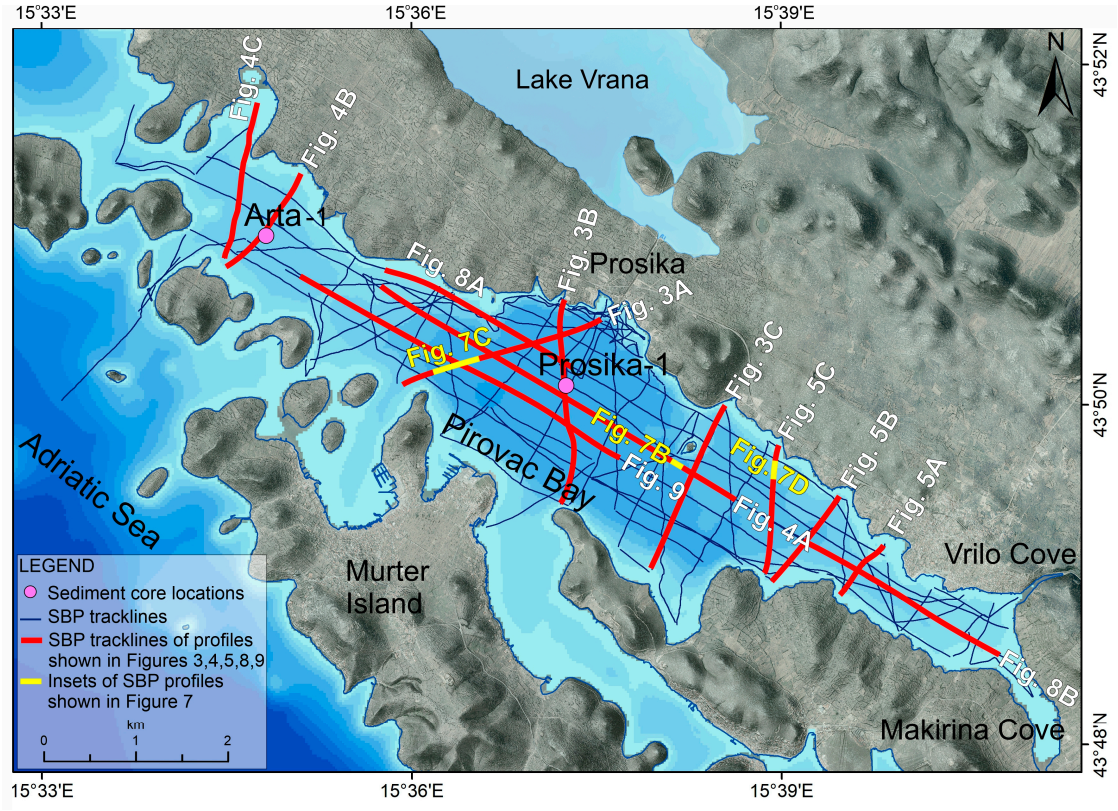


Figure 2. Sub-bottom profiler tracklines and sediment core locations.

A seismic survey was performed using an Innomar SES-2000 Light Plus (INNOMAR Technologie GmbH, Rostock, Germany) parametric sub-bottom profiler operating at high (100 kHz) and two low (6 and 8 kHz) frequencies. This setup provided a high vertical resolution and good penetration of the acoustic signal beneath the seafloor. The transducer was side-mounted on a small survey vessel that moved at a speed of approximately 3.5 knots. Vessel positioning was determined using Differential Global Positioning System navigation. Following acquisition, the data were converted from the Innomar RAW format to the SEGY format using SESconvert software (v2342_280225), and subsequently interpreted and analyzed using GeoSuite Allworks (v2024 R2) software. Differences in the reflection amplitude, continuity, and internal reflection configurations enabled discrimination between the seismic units [62].

3.2. Sediment Core Sampling

Two sediment cores were extracted from Pirovac Bay in 2011 (Figure 1B), using a 3 m-long and 60 mm-wide piston corer, mounted on a platform with a tripod and winches (UWITEC GmbH, Mondsee, Austria). The 7.45 m long Prosika-1 core (15°36′59.126″ E, 43°50′8.015″ N) was collected from the central part of the Bay at a water depth of 23 m (Figure 1B), whereas the 1.45 m long sediment core Arta-1 (15°34′33,778″ E, 43°51′1771″ N) was retrieved in the western part of Pirovac Bay at a water depth of 13 m (Figure 1B).

3.3. Laboratory Analyses

Sediment cores Prosika-1 and Arta-1 were sectioned into approximately 1.5 m long segments in the laboratory, subsequently split lengthwise and photographed. The sediment color was described using a Munsell color chart. The cores were then stored at +4 °C in a cold-storage facility until further analyses. A suite of analytical methods was used to analyze selected discrete samples, including grain-size, organic and inorganic geochemical, mineralogical and micropaleontological analyses. A detailed description of the methods and results, together with the complete multi-proxy dataset, is provided by Ilijanić et al. [45]. Here, we focus solely on the lithological variations throughout the cores (Table S1) and their chronological framework, which enabled a more complete assessment of the high-resolution seismic data.

Grain size analyses were performed using a Shimadzu Sald-2000 (Shimadzu Corporation, Kyoto, Japan) laser diffraction particle-size analyzer at the Croatian Geological Survey, allowing the measurement of particles ranging from 0.17 μm to 2 mm in size. A total of 83 samples from the Prosika-1 core and 26 samples from the Arta-1 core were analyzed. The acquired data were processed using GRADISTAT v8 [63].

The chronological framework of the sediment cores was constrained using nine Accelerator Mass Spectrometry (AMS) radiocarbon measurements, six in Prosika-1 and three in Arta-1 (Table S2) [45], and one cryptotephra layer [64]. AMS radiocarbon dating measurements were performed at Beta Analytic Inc. (Miami, FL, USA) and at the Radiocarbon Laboratory, Institute of Physics, Center for Science and Education, Silesian University of Technology (Gliwice, Poland). Marine shell samples were calibrated using the Marine20 calibration curve [65] with an appropriate marine reservoir correction, whereas freshwater shells and terrestrial plant material were calibrated using the IntCal20 calibration curve [66].

4. Results and Interpretation

Based on a detailed analysis of high-resolution seismic profiles, we identified various geomorphic features and distinct seismic stratigraphic units in the study area. Representative high-resolution seismic profiles are shown in Figures 3–5.

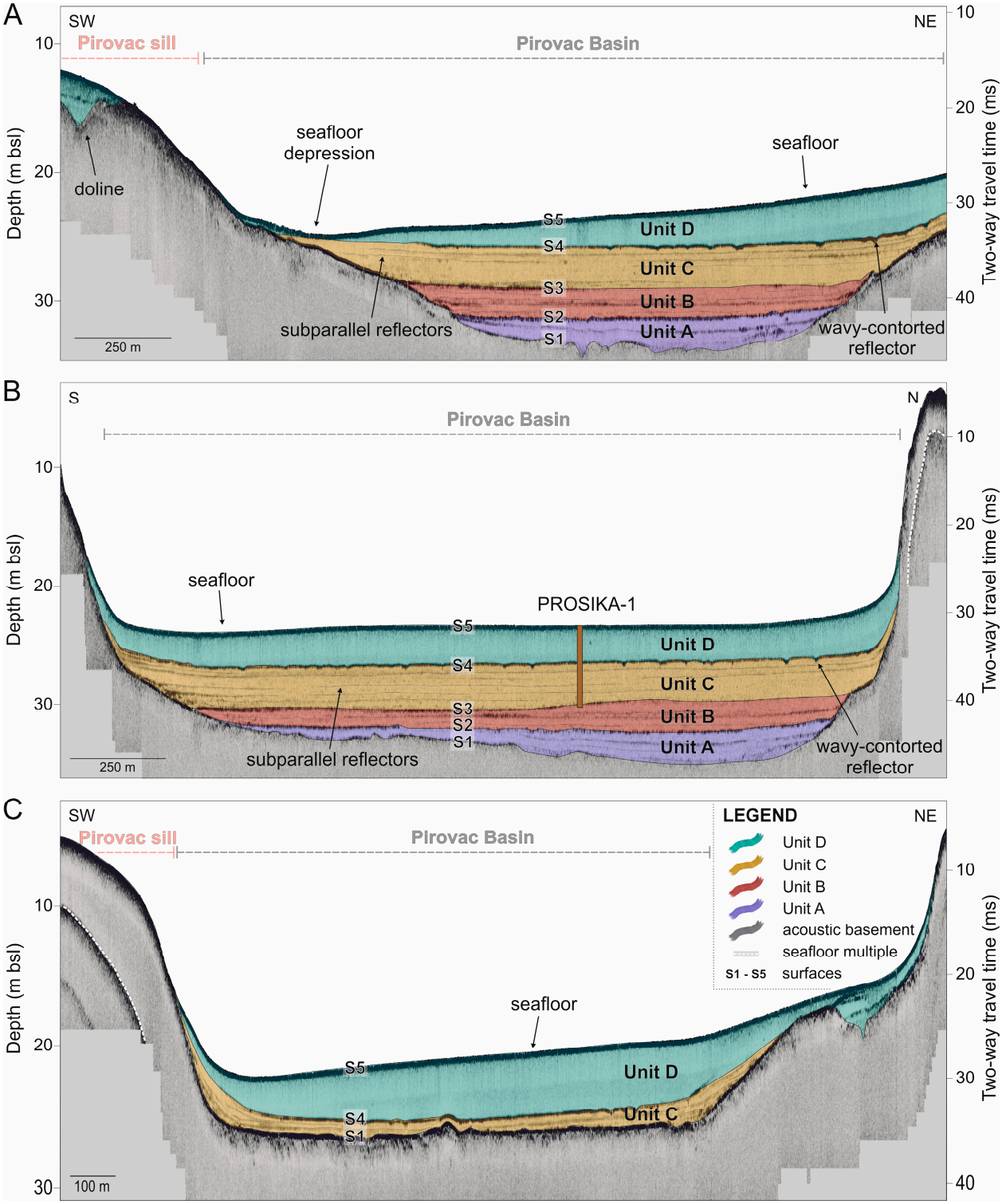


Figure 3. Interpreted high-resolution seismic profiles illustrating differentiated seismic units A–D, their bounding surfaces, and identified geomorphic features: (**A**) Profile PT50x_123512; (**B**) Profile PT012_155323; (**C**) Profile PT23x_103521. The profile locations are shown in Figure 2.

Sediment core data provided ground-truthing for remote sensing-derived data, enabling a more complete assessment of the observed seafloor and subsurface characteristics (Figure 6).

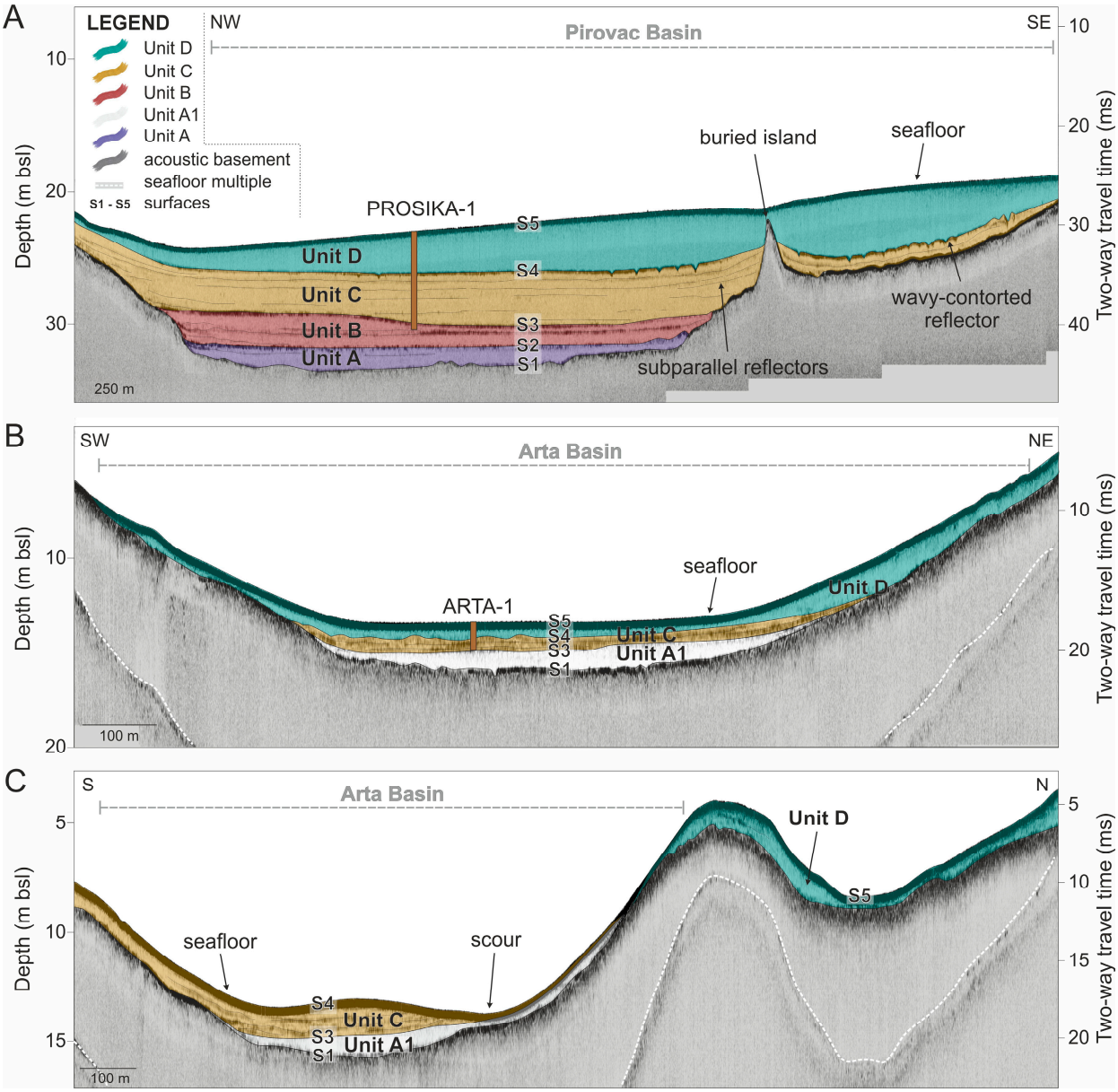


Figure 4. Interpreted high-resolution seismic profiles illustrating differentiated seismic units A–D, their bounding surfaces, and identified geomorphic features: (**A**) Profile PP1_094116; (**B**) Profile PT20x_172905; (**C**) Profile PT21_142550. Sediment cores Prosika-1 and Arta-1 are also shown in the figure. The profile locations are shown in Figure 2.

4.1. Seafloor and Subsurface Morphological Features

The acquired data revealed the existence of two depressions within the Pirovac Bay area, as previously discussed by Ilijanić et al. [45]. The first depression is located in the southeastern part of the bay (hereafter referred to as the Pirovac Basin), whereas the second depression occupies the northwestern part (hereafter referred to as the Arta Basin) (Figures 3 and 4). Both depressions are clearly delineated in the high-resolution seismic profiles as enclosed morphological lows through which the acoustic signal does not penetrate (i.e., acoustic basement–surface S1) and are bounded by relatively steep margins (Figures 3 and 4). The larger, elongated, and morphologically more complex depression, the Pirovac Basin, extends over approximately 5.8 km and has a width of approximately 2.2 km. Its base reaches a maximum depth of ~35 m below the present sea level (bsl) (46.5 ms two-way travel time (TWT)). It is infilled with a sedimentary succession

up to 11.5 m thick. In contrast, the Arta Basin is smaller in both lateral extent and depth, with dimensions of approximately 1.7 × 1.4 km. It contains a sedimentary infill reaching a maximum thickness of 2.8 m, indicating limited depositional space compared to the Pirovac Basin. The two basins are separated by a bathymetric high (i.e., Pirovac sill), with a maximum depth of 8 m bsl (Figure 7). This sill is laterally continuous and forms a prominent submerged morphological barrier between the two depressions, connecting the Dalmatian mainland with nearby islands. It is observed on high-resolution seismic profiles as a pronounced reflector S1 on the present-day seafloor, through which the acoustic signal does not penetrate (Figure 7). The Arta Basin is separated from the Adriatic Sea by a second sill (Arta sill) with a maximum depth of approximately 6 m bsl, located northwest of the Arta Basin (Figure 7).

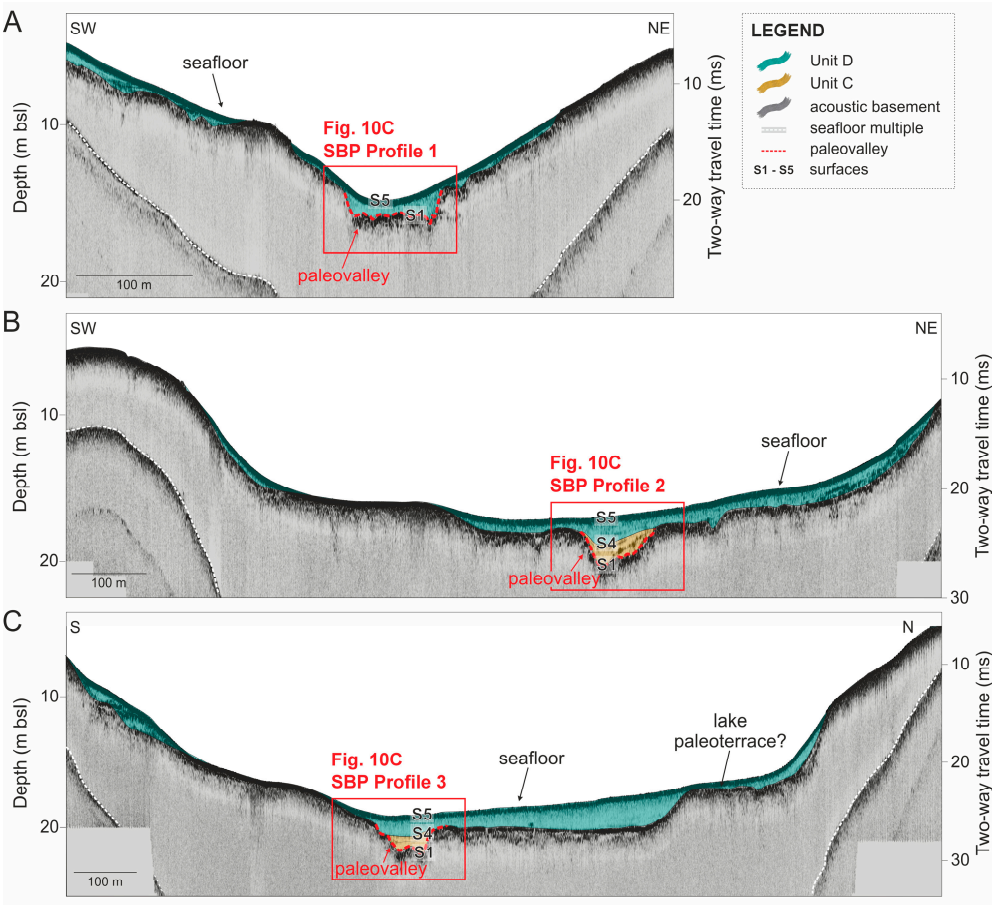


Figure 5. Interpreted high-resolution seismic profiles illustrating differentiated seismic units C and D, their bounding surfaces and identified submerged and buried paleovalley: (**A**) Profile PT05_132546; (**B**) Profile PT07_134439; (**C**) Profile PT08_135730. The profile locations are shown in Figure 2.

In addition to these major morphological features, a prominent erosional terrace cut into the acoustic basement was identified on several high-resolution profiles from the Pirovac Basin (Figures 5 and 7A,D). This terrace is laterally incised into the acoustic basement and is found at a depth of approximately 17 m bsl (22 ms TWT). A submerged and partly buried island was also recognized in the Pirovac Basin, interpreted as a morphological continuation of the adjacent Sustipanac Island (Figures 4 and 7A,B). The island extends approximately 500 m and has a maximum width of 230 m. The maximum elevation of the submerged island reaches 11 m bsl, rising 8 m above the surrounding seafloor. In high-resolution seismic profiles, it is characterized by a continuous and steep acoustic reflector S1 through which acoustic waves do not penetrate the subsurface (i.e., the acoustic basement). It is partly draped by sedimentary deposits (~1 m thick), indicating a preexist-

ing topographic high. Furthermore, in the southeastern part of Pirovac Bay, the acoustic basement is locally incised by a well-defined buried paleovalley, which was infilled with up to 5.2 m of sediments (Figure 5). This feature is observed in high-resolution seismic data as an irregular, concave-up S1 reflection at the base of the sedimentary succession (Figure 5). The maximum incision reached approximately 21.2 m (28.4 ms TWT), whereas the paleovalley extends for approximately 2.7 km along the profiles and varies in width between 30 and 140 m (Figure 7A). A seafloor depression is observed adjacent to the Pirovac and Arta sills and along the southern coastline of the bay (Figure 7). In the Pirovac Basin, the depression extends approximately 2 km along the bay, reaches a maximum width of approximately 800 m adjacent to the sill, and is incised up to 2.5 m below the surrounding seafloor (Figure 3). A similar feature was also observed in the Arta Basin, with a length of approximately 1.2 km, width of 640 m, and maximum depth of 0.75 m. The erosional character of this feature is inferred from the truncation of the underlying reflectors by the seafloor reflector (Figure 4C), supporting the interpretation of the depression as an erosional scour. Finally, several profiles revealed the presence of smaller karst depressions (i.e., dolines) in the study area (Figures 3 and 7).

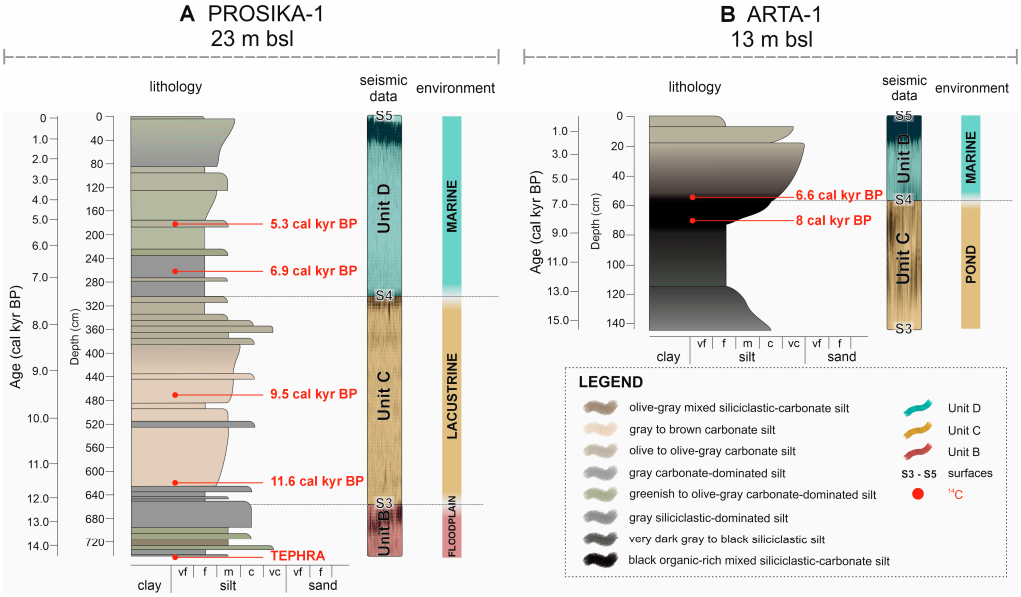


Figure 6. Lithological variations observed in sediment cores Prosika-1 (**A**) and Arta-1 (**B**) and their correlation with interpreted high-resolution seismic data. The silt and sand fractions were subdivided into vf (very fine), f (fine), m (medium), c (coarse), and vc (very coarse). The tephra layer corresponds to the NYT [61].

4.2. Seismic Stratigraphy

The acoustic signal penetrated up to approximately 35 m bsl (46.5 ms TWT), allowing detailed imaging of the subsurface. We distinguished the acoustic basement and overlying sedimentary infill of Pirovac Bay (Figures 3, 4 and 7). The acoustic basement is identified as a prominent, irregular, laterally continuous high-amplitude reflection S1, within which most of the previously described geomorphological features are developed and which forms the base of the sedimentary succession. Overall, four distinct seismic units were identified and described in the Pirovac Basin, from the oldest at the base to the youngest at the top of the succession (Units A to D) (Figures 3 and 4). However, only three units were recognized in the Arta Basin (Units A1, C, and D) (Figure 4). Sediment thickness exhibits considerable spatial variability and does not increase towards the deepest part of the Pirovac Basin. High-resolution seismic profiles also revealed distinct, elongated plumes ascending from the seafloor toward the upper part of the water column (Figure 8).

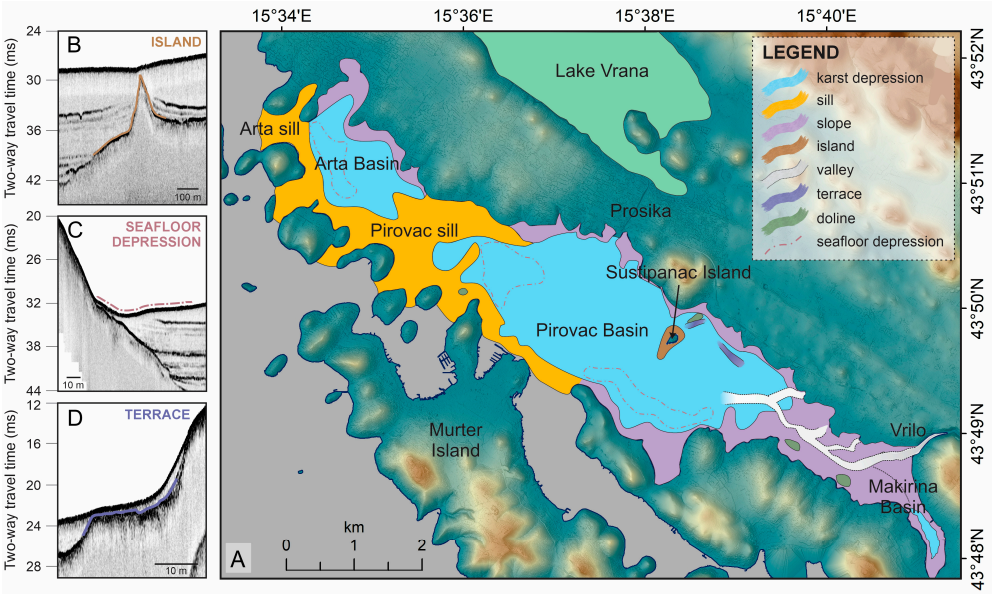


Figure 7. (**A**) Geomorphological map of the study area derived from the interpretation of the high-resolution seismic profiles. The profile locations (**B**–**D**), illustrating some of the differentiated geomorphological features, are shown in Figure 2.

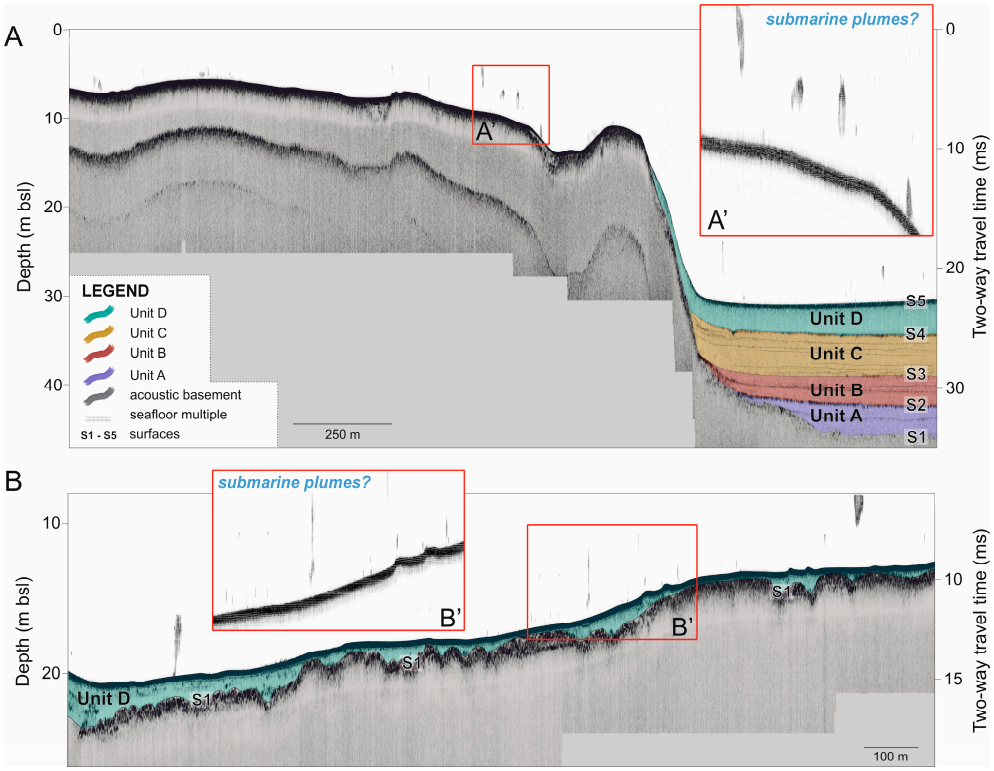


Figure 8. Interpreted high-resolution seismic profiles illustrating differentiated seismic units A–D, their bounding surfaces, and potential submarine groundwater discharge in the form of submarine plumes: (**A**) Profile PP4_111946; (**B**) Profile CL_144744. The profile locations are shown in Figure 2.

Seismic Unit A is the lowermost unit within the sedimentary infill of the Pirovac Basin, characterized by a few sub-parallel, moderate-amplitude reflections with limited lateral continuity (Figures 3 and 4). The unit conformably drapes the top of the acoustic basement and reaches a maximum thickness of 1.9 m. It is spatially restricted to the deepest part of the Pirovac Basin and is absent in other investigated areas. The acoustic basement of the Arta

Basin is covered by Seismic Unit A1 deposits, which are characterized by a reflection-free acoustic pattern and a maximum thickness of 1.8 m (Figure 4).

An unconformable, high-amplitude surface S2 separates Unit A from Unit B (Figures 3 and 4). The latter unit comprises several moderate-amplitude, laterally discontinuous, and sub-parallel reflections that are locally truncated by the overlying S3 reflector. Externally, Unit B displays an apparent mounded geometry, which may also reflect post-depositional erosion of the sediments. Its maximum thickness of approximately 1.6 m was observed in the northern part of the Pirovac Basin, whereas the unit progressively thins towards the southeast.

Seismic Unit C consists of laterally discontinuous, sub-parallel internal reflections of low-to-moderate amplitude (Figures 3 and 4). It unconformably overlies the underlying seismic units. In the Pirovac Basin, Unit C exhibits a vertical change in seismic character, from being predominantly acoustically transparent with several low-amplitude reflections in its lower part to more continuous, moderate-amplitude reflections upward. The unit is separated from the overlying seismic unit by a wavy-contorted reflector, S4 (Figure 3). Unit C is the thickest in the Pirovac Basin, reaching up to 4 m, whereas it is considerably thinner in the Arta Basin, with a maximum thickness of approximately 1 m (Figures 3 and 4).

The topmost unit (Unit D) is generally characterized by a reflection-free acoustic pattern (Figures 3–5). Externally, it exhibits a draping geometry and overlies both the acoustic basement and underlying seismic units. The upper boundary of Unit D corresponds to the present seafloor. The seafloor reflector (S5) occasionally cuts Unit C unconformably in the area adjacent to the Pirovac and Arta sills (Figure 4). Unit D is present across the investigated area and occurs in both basins. It is generally absent only in areas where the acoustic basement is exposed at the seafloor (Figures 3–5). The unit has a maximum thickness of 5 m in the southeastern part of the Pirovac Basin, whereas its thickness decreases northward and westward. The thickness of Unit D is significantly reduced in the Arta Basin (Figure 4).

4.3. Lithology and Chronology of Sediment Cores

The basal part of the Prosika-1 core (745–660 cm), deposited between >14 cal kyr BP and 12.4 cal kyr BP, predominantly consists of gray to olive-gray, medium- to coarse-grained carbonate-dominated silt (Figure 6). This interval is characterized by the highest sand content within the core, whereas clay is almost absent (Table S1). The overlying interval (660–300 cm), spanning the period between 12.4 cal kyr BP and 7.3 cal kyr BP, is dominated by gray to brown carbonate sediments, with silt as the prevalent grain-size fraction (Figure 6). Clay is consistently present in subordinate amounts, whereas the sand content is generally low (Table S1). The uppermost section of the Prosika-1 core (300–0 cm), deposited from 7.3 cal kyr BP to the present, is composed of fine-grained, olive-gray, carbonate-dominated sediments (Figure 6). Silt is the dominant fraction, although clay is also abundant, and the sand content is negligible (Table S1).

The lower part of the Arta-1 core (145–58 cm), spanning the period between 15.5 cal kyr BP and 6.8 cal kyr BP, predominantly consists of gray to black siliciclastic silt (Figure 6). The clay content is relatively high, whereas the sand content is low (Table S1). Larger clasts of varying sizes were also observed. The top of the core (58–0 cm), deposited since 6.8 cal kyr BP, is characterized by olive-gray carbonate silt (Figure 6) with abundant clay, along with an increase in sand content upcore (Table S1).

5. Discussion

5.1. Morphological Controls on the Evolution of Coastal Karst Basins

A variety of morphological features were identified in the Pirovac Bay subsurface, including larger depressions, dolines, sills, a terrace, an island, a valley, and scours (Figure 7).

Many of these submerged landforms are likely a product of the extensive karstification that has shaped the eastern Adriatic coast and governed the region's long-term geomorphological evolution [47,67].

Both the Pirovac and Arta depressions can be interpreted as karstic in origin and can, therefore, be classified as karst depressions (Figure 7). The study area is dominated by limestone and dolomite [54,58], which are highly susceptible to karstification. Many Mediterranean karst areas are widely considered to have evolved during the Miocene under subaerial conditions [28,68]. During the Pleistocene, repeated sea-level lowstands promoted additional karstification through the subaerial exposure of the shallow shelf [11]. We hypothesize that one possible explanation for the Pirovac depression preserving only the most recent sediments (i.e., post-LGM sediment succession) [45] is that the basin either formed relatively recently, possibly even after the Last Interglacial, or experienced significant sediment mobilization and/or erosion. If the basin had formed earlier, a thicker sedimentary succession would be expected, as documented in other coastal karst basins along the eastern Adriatic coast [67] and in Mediterranean karst lakes [69]. An alternative explanation for the relatively thin sediment succession in the Pirovac Bay includes sediment transport through subsurface karst pathways (i.e., swallow holes). Swallow holes (ponors) may eventually be infilled and plugged by remobilized sediments, a process commonly observed in karst systems [4]. The timing and exact mechanisms that led to the formation of depressions thus remain unanswered and require further investigation.

The recognition of morphological barriers (i.e., sills) and the estimation of their depths is of high importance, as these features govern the marine inundation or isolation of depressions in response to relative sea-level oscillations [40]. Our survey indicated that the studied basins were separated from the Adriatic Sea by two sills (Figure 7). Direct marine flooding of the depressions could only have occurred once the relative sea level exceeded sill depths of approximately 6 m bsl (Arta sill) and 8 m bsl (Pirovac sill), corresponding to the Middle Holocene transgression. However, in karst settings, hydrological connectivity is not exclusively controlled by surface morphology [4,70]. Consequently, the onset of marine influence within coastal karst basins may have occurred before the physical transgression of the sills, complicating the interpretation of sedimentary records based solely on bathymetric highs. The subsurface intrusion of marine water into coastal karst basins has been previously documented and elaborated in detail by Surić et al. [27] and van Hengstum et al. [26].

5.2. Late Quaternary Evolution of Depositional Environments

The karst depressions with sills identified in Pirovac Bay are comparable to dolines in terms of their origin and morphology, although they are typically larger and more complex [67]. Such depressions often act as natural sediment traps [21,71], thereby generating accommodation space required for the establishment of Quaternary depositional environments (Figure 9).

The results allowed for the identification of distinct depositional phases within the Late Glacial–Holocene sediment succession, corresponding to seismic Units A to D and representing distinct sedimentary regimes and environmental conditions (Figure 9). The reconstructed phases comprise: (a) a potentially subaerial environment (Unit A), (b) a fluvial and floodplain environment (Unit B), (c) a lacustrine environment (Unit C), and (d) a fully marine environment (Unit D). These phases document the environmental transformation of the basins from subaerial karst depressions to a single marine embayment that evolved during the post-glacial relative sea-level rise (Figure 9). Similar environments have also been documented in other karst settings worldwide [36,72,73] and in the Adriatic

Sea [40,41], although their depositional successions differ somewhat from that found in the present study.

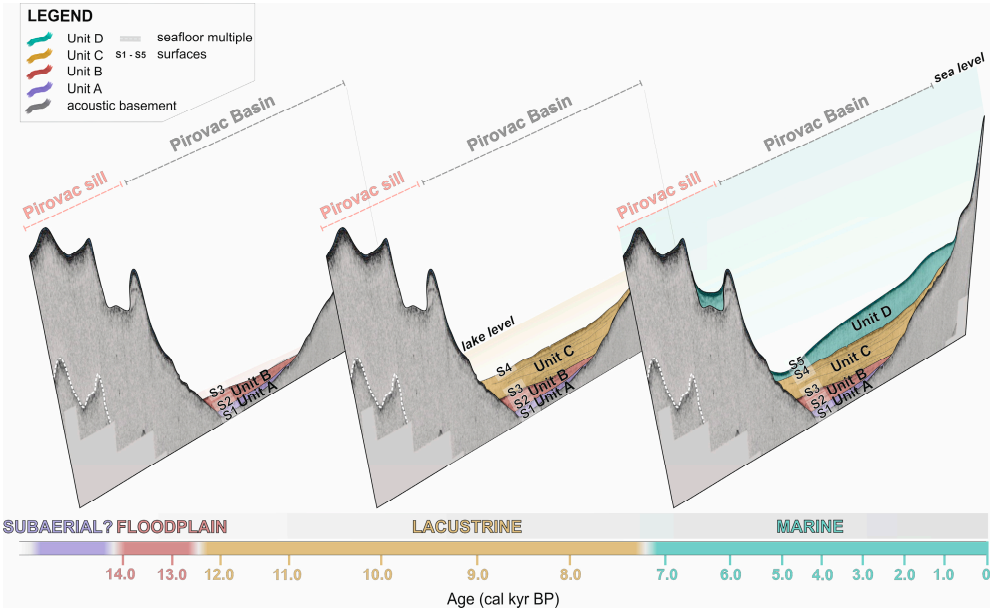


Figure 9. Late Glacial to Holocene evolutionary model of the Pirovac Basin.

(a) Potentially subaerial environment (Unit A)

Without sediment core data, the reliable identification of the depositional environment is challenging, and any interpretation of Unit A remains hypothetical. However, studies of karst depressions along the eastern Adriatic coast, both offshore and onshore [40,41,74], often show their initial infilling by soil, which could act as a seal in porous karst basins and facilitate the subsequent water accumulation. Accordingly, it is highly plausible that the basal part of the Pirovac Basin succession is covered by soil (Figure 9). A comparable interpretation may also be applied to the Arta Basin (Unit A1). The age of these units is constrained to >14 cal kyr BP in the Pirovac Basin and >15 cal kyr BP in the Arta Basin based on chronological data derived from sediment cores and overlying units (Figure 6). The relative sea level during the period before 14–15 cal kyr BP was significantly lower than at present [75], which could have enabled the development of a subaerial environment within the basins.

(b) Fluvial and floodplain environment (Unit B)

Following the deposition of Unit A, a large part of the Pirovac Basin transformed into a floodplain environment (Figure 9), as previously inferred from multi-proxy sediment core data [45], representing a transitional setting influenced by intermittent subaerial exposure and flooding. In high-resolution seismic data, we also identified erosional surface S2 within the basin (Figure 3), and a submerged and buried paleovalley incised into the karstified basement in the southeastern part of the study area (Figure 5), supporting the formation of a fluvial environment. This landform, with a maximum incision of 21.2 m bsl (28.4 ms TWT), is now completely infilled by sediments and is likely a relict of a subaerial drainage system formed during the period of lower sea level. The valley extends on land, where it represents an inactive remnant of this flow, also recognized in Light Detection and Ranging (LiDAR) data obtained as part of the 'Multisensor Aerial Survey of the Republic of Croatia' project (Figure 10). The morphology of the onland dry valley closely resembles that observed in high-resolution seismic profiles (Figure 10). This feature was not identified in the previous analysis of the study area, which was based solely on sediment core data [45].

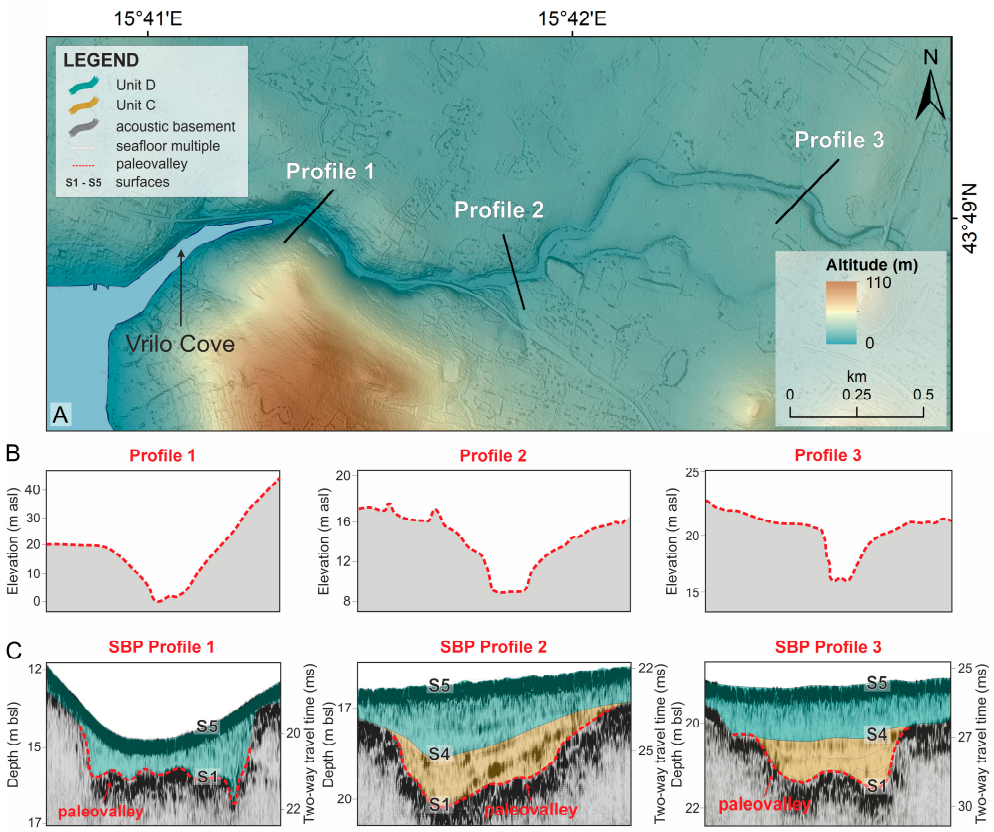


Figure 10. (**A**) Digital elevation model of the wider study area obtained from LiDAR data (Digital orthophoto LiDAR (2022/23) (https://geoportal.dgu.hr/ (accessed on 21 July 2026))); (**B**) Comparison of onshore dry fluvial valley profiles, and (**C**) submerged offshore fluvial valley recognized in high-resolution seismic data. The complete high-resolution seismic profiles corresponding to the insets are presented in Figure 5, and their locations are shown in Figure 2.

The ancient Vrilo River, now only present as the coastal spring Vrilo (Figure 1B), presumably had a major role in the formation of the fluvial valley and floodplain environment in the Pirovac Basin. It is difficult to constrain the exact timing and duration of this environmental phase in this area. Sediment core data indicate that floodplain conditions commenced before 14 cal kyr BP and persisted until 12.4 cal kyr BP. Submerged post-LGM fluvial environments have also been investigated and identified along the eastern [50,67,76] and western [51,77] Adriatic coasts. However, the formation of the observed fluvio-karst valley probably involved long-term, multi-phase evolution spanning hundreds of thousands of years, consistent with the development of fluvio-karst systems over Quaternary timescales [32]. Accordingly, the incised paleovalley was likely active during several sea-level lowstands. The Pirovac sill acted as a barrier to fluvial flow, most probably causing this river to sink underground through a ponor zone, which is a characteristic of karst fluvial systems in which drainage alternates between surface and subsurface pathways [70]. The fact that this drainage pathway is no longer active, despite being strongly controlled by the existing geomorphology, indicates that significant changes in the hydrological regime have occurred since its formation. This finding also provides evidence of fluvio-karst processes occurring in the region, in contrast to many other carbonate terrains, where fluvial environments are poorly developed or completely absent [26,71].

(c) Lacustrine environment (Unit C)

Unit C records the transition from a preceding fluvially dominated environment to a lacustrine system (Figure 9), based on sediment core data [45]. High-resolution seismic profiles reveal predominantly sub-parallel seismic reflections with an aggradational

stacking pattern (Figures 3 and 4), whereas sedimentological analyses indicate the gradual evolution of the lake from freshwater to brackish-water conditions [45]. The data further show that between approximately 12.4 cal kyr BP and 7.3 cal kyr BP, the Pirovac Basin remained isolated from direct marine influence. Fluvial conditions likely persisted in the southeasternmost part of the basin, where the incised paleovalley is only infilled by the overlying Unit D deposits (Figure 10).

The lacustrine succession, reaching a thickness of approximately 4 m, lacks pronounced erosional surfaces (Figure 3), suggesting continuous sedimentation under relatively stable or gradually rising lake levels. Similarly, the absence of retrogradational or progradational features indicates that major lake-level fluctuations did not occur. The lake level probably never exceeded the elevation of the Pirovac sill to overflow into the Arta Basin, as lacustrine deposits were not identified in this basin [45]. Possible wave-cut terraces recognized along the southeastern margins of the paleolake may indicate phases of lake-level stillstands (Figure 7). However, their formation in a carbonate substrate likely required prolonged periods of stable lake levels [78], which does not support the hypothesis that this depression formed relatively recently. Based on the depth difference between the terraces (~17 m bsl) and the base of the lacustrine succession (~30 m bsl), the paleolake is inferred to have been relatively shallow, with a maximum depth of approximately 13 m, similar to present-day Lake Vrana near Biograd na Moru. Nevertheless, the basin geomorphology (i.e., sill depth) indicates that the lake may have reached a maximum depth of 22 m.

Several factors played a key role in the evolution of the paleolake in the Pirovac Basin. The period during which the lake existed coincided with a generally wetter climatic phase in the Adriatic region [79–81], when increased precipitation likely enhanced surface runoff and drainage through the southeastern valley. The presence of a ponor (i.e., swallow hole) within the basin may also affect lake development [4,70]. If plugged by sediments, it would reduce subsurface drainage and promote water retention. Nevertheless, groundwater dynamics probably exerted a dominant control on lake development and hydrology in this karst setting. Relative sea-level rise during the Holocene [8,75] caused a corresponding rise in groundwater levels, facilitating the establishment of the coastal lake. As the sea level continued to rise, brackish conditions gradually developed owing to the subsurface intrusion of marine waters through the karst conduit network, a process well documented in coastal karst environments [26]. Consequently, the final phase of lake evolution was characterized by an increasing marine influence in an enclosed basin.

The Pirovac paleolake is the youngest Holocene lake along the eastern Adriatic coast that has been submerged by postglacial sea-level rise, with lacustrine sedimentation lasting almost 5000 years. Two coastal lakes, Pirovac paleolake and adjacent Lake Vrana near Biograd na Moru, Croatia's largest lake, may have coexisted during the Middle Holocene. Together, these coastal systems likely represented important freshwater environments along the eastern Adriatic coast [82]. Previous studies have shown that submerged karst lakes were widespread in the region during periods of lower sea levels and were subsequently inundated and covered by marine deposits [18,40,79].

(d) Fully marine environment (Unit D)

The topmost Unit D overlies the entire sedimentary succession and records the transition to modern marine conditions (Figure 9). The onset of this phase was dated to 7.3 cal kyr BP in the Prosika-1 core and to 6.8 cal kyr BP in the Arta-1 core (Figure 6), indicating that the Pirovac and Arta basins functioned predominantly as marine environments for most of the Holocene. This paleoenvironmental transition likely resulted from the Holocene transgression, when rising sea levels exceeded the Pirovac and Arta sills, which had previously maintained the surface isolation of the basins from direct marine influence, despite continued subsurface connectivity through the karst network. At the time of transgres-

sion, relative sea level is inferred to be ~7–9 m lower than at present [75,83], enabling the establishment of a fully marine sedimentation regime.

High-resolution seismic data additionally revealed erosional surfaces. In particular, the seafloor reflector (S5) truncates older deposits adjacent to both sills, suggesting substantial reworking and sediment redistribution following marine inundation (Figures 3 and 4). These erosional features likely reflect intensified bottom-current activity associated with morphological constrictions created by sills [84], which may have accelerated local circulation and sediment erosion. Furthermore, hydrodynamic processes may have been enhanced by submarine groundwater discharge through the subsurface karst network, potentially generating turbulence and density-driven circulation near the seafloor. These observations could indicate that both basin morphology and karst-controlled hydrology strongly influenced sediment dynamics after the establishment of modern marine conditions.

5.3. Submarine Groundwater Discharge

Coastal karst aquifers are important freshwater reservoirs, with groundwater commonly discharging through coastal and submarine springs owing to complex subsurface hydrological connectivity [24,28,85]. Such features are characteristic of the investigated Pirovac Bay, where many coastal karst springs have been identified along the eastern coastline toward freshwater Lake Vrana near Biograd na Moru (Figure 1B). In addition, the distinct plumes observed in the water column in the study area may represent submarine groundwater discharge. They appear as vertically elongated irregular plumes extending from the seafloor to the sea surface in parametric sub-bottom profiler data (Figure 8). Although a biological origin cannot be entirely excluded, their predominantly narrow, elongated morphology differs from the broader and more diffuse acoustic signatures typically associated with fish schools. Likewise, marine vegetation usually produces bottom—attached reflections, unlike the plumes observed here (Figure 8). Furthermore, their elongated geometry is consistent with the expected behavior of freshwater ascending through denser marine water. The plumes may have originated in the karst basement and penetrated the sedimentary succession (Figure 8). If this interpretation is correct, the identified features may indicate that karst-controlled groundwater discharge is currently an active process within the basins. Further support for this interpretation is provided by the occurrence of freshwater ostracod assemblages alongside marine species in post-transgression sediments of the Prosika-1 sediment core [45].

Considering the growing interest in submarine fresh groundwater resources [29,86], driven by climate change, rising water demand, and the scarcity of potable water, the identification of alternative locations and methods for extracting this vital resource has become an increasingly important research priority in recent years. In particular, karst regions are particularly relevant due to their distinct hydrogeological characteristics and potential to store substantial quantities of freshwater. Emerging technologies may facilitate the capture of such water [87,88]. However, the results of our study suggest that groundwater discharge within the investigated area occurs predominantly through diffuse seepage, potentially complicating its identification, characterization, and exploitation.

6. Conclusions

This study provides new insights into the depositional history of coastal karst basins through an integrated analysis of high-resolution seismic profiles and sediment cores, and highlights the interactions among karst geomorphology, hydrological regimes, sedimentary processes, and relative sea-level dynamics that governed the basin evolution.

Geomorphological features typical for karst settings (i.e., karst depressions) provided the accommodation space and, consequently, strongly influenced the development of

depositional environments in the Pirovac Bay. The evolutionary model documents the transition from subaerial, floodplain-fluvial, lacustrine, and finally marine environmental conditions that occurred since the Late Glacial. Our findings further showed that coastal karst basins do not transition abruptly from terrestrial to marine conditions; instead, they evolve through hydrologically transitional phases mediated by subsurface karst connectivity. In this context, the sill exerted only partial control over the environmental evolution and marine inundation of the Pirovac and Arta basins. Although the investigated basins are characterized by enclosed morphologies, the data indicate that erosional processes can influence these settings. In particular, erosional scours identified adjacent to the sills could be generated by intensified bottom currents associated with flow constrictions.

Most models describing the evolution of coastal karst basins have largely overlooked the possibility that more complex depositional and geomorphological systems may develop within such settings. In particular, the formation of fluvio-karst environments within coastal karst basins has rarely been considered. Our findings demonstrate that fluvio-karst can develop within coastal basins and may represent an important part of their Quaternary evolution. These observations also show that submerged karst landscapes are considerably more diverse than is currently reflected in existing classification schemes that often lack descriptors that are specific to submerged karst features.

The obtained data further support subsurface hydrological connectivity between the investigated coastal karst basins and inland freshwater sources such as Lake Vrana near Biograd na Moru. In the context of ongoing climate change and increasing freshwater scarcity, understanding these hydrological interactions is particularly important. Furthermore, the evolutionary model proposed for Pirovac Bay may provide a valuable framework for assessing potential future environmental changes in adjacent karst settings, including Lake Vrana near Biograd na Moru, under scenarios of continued sea-level rise.

Supplementary Materials: The following supporting information can be downloaded at: https://www.mdpi.com/article/10.3390/jmse14151360/s1. Table S1: Grain-size analyses data [45]; Table S2: Radiocarbon dating results [45].

Author Contributions: Conceptualization, D.B.; Methodology, D.B., O.H. and N.I.; Software, D.B. and O.H.; Formal analysis, D.B.; Investigation, D.B., O.H. and N.I.; Resources, S.M. and N.I.; Writing—original draft, D.B. and O.H.; Writing—review and editing, D.B., O.H., N.I., and S.M.; Visualization, D.B. and O.H.; Supervision, S.M. and N.I.; Project administration, S.M. and N.I.; Funding acquisition, S.M. and N.I. All authors have read and agreed to the published version of the manuscript.

Funding: This work was supported by the Croatian Science Foundation project "Lost Lake Landscapes of the Eastern Adriatic Shelf" (LoLADRIA; HRZZ-IP-2013-11-9419) and "Sediments be-tween source and sink during a late Quaternary eustatic cycle: the Krka River and the Mid Adriatic Deep System" (HRZZ IP-04-2019-8505). This research was conducted in the scope of the internal research project "PLATE" at the Croatian Geological Survey, funded by the National Recovery and Resilience Plan 2021–2026 of the European Union–NextGenerationEU, and monitored by the Ministry of Science and Education of the Republic of Croatia. We thank Innomar Technologie GmbH for granting us the equipment (SES-2000 sub-bottom profiler system) and technical support for the survey.

Data Availability Statement: All data are available upon request and in the Supplementary Tables.

Acknowledgments: The authors would like to thank Peter Huembs of Innomar Technologie GmbH for his technical support during fieldwork. We would like to thank the editor and four anonymous reviewers for their expert, insightful, and constructive comments, which greatly improved the manuscript.

Conflicts of Interest: The authors declare no conflicts of interest.

Abbreviations

The following abbreviations are used in this manuscript:

AMS	Accelerator Mass Spectrometry
asl	above the present sea level
bsl	below the present sea level
NYT	Neapolitan Yellow Tuff
LGM	Last Glacial Maximum
TWT	Two-way travel time

References

1. Bondesan, A.; Meneghel, M.; Sauro, U. Morphometric Analysis of Dolines. *Int. J. Speleol.* **1992**, *21*, 1–55. [CrossRef]
2. Margiotta, S.; Marini, G.; Fay, S.; D'onghia, F.M.; Liso, I.S.; Parise, M.; Pinna, M. Hydro-stratigraphic Conditions and Human Activity Leading to Development of a Sinkhole Cluster in a Mediterranean Water Ecosystem. *Hydrology* **2021**, *8*, 111. [CrossRef]
3. Švara, A.; Mihevc, A.; Zupan Hajna, N. Active and Relict Contact Karst Morphological Forms of the Slavina Corrosional Plain. *Acta Carsologica* **2022**, *51*, 21–41. [CrossRef]
4. Ford, D.C.; Williams, P. *Karst Hydrogeology and Geomorphology*; Wiley: London, UK, 2007.
5. Holtvoeth, J.; Vogel, H.; Wagner, B.; Wolff, G.A. Lipid Biomarkers in Holocene and Glacial Sediments from Ancient Lake Ohrid (Macedonia, Albania). *Biogeosciences* **2010**, *7*, 3473–3489. [CrossRef]
6. Wagner, B.; Wilke, T. Preface "Evolutionary and Geological History of the Balkan Lakes Ohrid and Prespa". *Biogeosciences* **2011**, *8*, 995–998. [CrossRef]
7. Ivkić Filipović, I.; Ilijanić, N.; Miko, S.; Hasan, O.; Brunović, D.; Kordić, B.; Barudžija, U.; Sladović, Ž. Late Quaternary Geomorphology and Sedimentary Processes in the Prološko Blato Karst Wetland (Imotsko Polje, Croatia). *Geomorphology* **2025**, *482*, 109765. [CrossRef]
8. Lambeck, K.; Antonioli, F.; Purcell, A.; Silenzi, S. Sea-Level Change along the Italian Coast for the Past 10,000 Yr. *Quat. Sci. Rev.* **2004**, *23*, 1567–1598. [CrossRef]
9. Lambeck, K.; Rouby, H.; Purcell, A.; Sun, Y.; Sambridge, M. Sea Level and Global Ice Volumes from the Last Glacial Maximum to the Holocene. *Proc. Natl. Acad. Sci. USA* **2014**, *111*, 15296–15303. [CrossRef] [PubMed]
10. Furlani, S.; Ninfo, A.; Zavagno, E.; Paganini, P.; Zini, L.; Biolchi, S.; Antonioli, F.; Coren, F.; Cucchi, F. Submerged Notches in Istria and the Gulf of Trieste: Results from the Geoswim Project. *Quat. Int.* **2014**, *332*, 37–47. [CrossRef]
11. Surić, M. Submarine Karst of Croatia—Evidence of Former Lower Sea Levels Podmorski Kras Na Hrvaškem—Dokaz O Nekdanji Nižji Morski Gladini. *Acta Carsologica* **2002**, *31*, 89–98.
12. Surić, M.; Korbar, T.; Juračić, M. Tectonic Constraints on the Late Pleistocene-Holocene Relative Sea-Level Change along the North-Eastern Adriatic Coast (Croatia). *Geomorphology* **2014**, *220*, 93–103. [CrossRef]
13. Faivre, S.; Fouache, E.; Ghilardi, M.; Antonioli, F.; Furlani, S.; Kovačić, V. Relative Sea Level Change in Western Istria (Croatia) during the Last Millennium. *Quat. Int.* **2011**, *232*, 132–143. [CrossRef]
14. Antonioli, F.; Furlani, S.; Montagna, P.; Stocchi, P. The Use of Submerged Speleothems for Sea Level Studies in the Mediterranean Sea: A New Perspective Using Glacial Isostatic Adjustment (GIA). *Geosciences* **2021**, *11*, 77. [CrossRef]
15. Lončar, N.; Faivre, S.; Miklavič, B.; Baričević, M. Tidal Dynamics in Coastal Karst Caves: Contributions to Coastal Hydrology and Historical Relative Sea-Level Reconstruction Using Phreatic Overgrowths on Speleothems in the Eastern Adriatic. *Hydrol. Process.* **2025**, *39*, e70148. [CrossRef]
16. Bard, E.; Antonioli, F.; Silenzi, S. Sea-Level during the Penultimate Interglacial Period Based on a Submerged Stalagmite from Argentarola Cave (Italy). *Earth Planet. Sci. Lett.* **2002**, *196*, 135–146. [CrossRef]
17. Surić, M.; Richards, D.A.; Hoffmann, D.L.; Tibljaš, D.; Juračić, M. Sea-Level Change during MIS 5a Based on Submerged Speleothems from the Eastern Adriatic Sea (Croatia). *Mar. Geol.* **2009**, *262*, 62–67. [CrossRef]
18. Schmidt, R.; Pugliese, N.; Müller, J.; Szeroczyriska, K.; Bogner, D.; Melis, R.; Kamenik, C.; Bari, A.; Danielopol, D.L. Palaeoclimate, Vegetation and Coastal Lake Development, from the Pleniglacial until Early Holocene, in the Northern Adriatic Valun Bay (Isle of Cres, Croatia). *Quat. J. Quat. Sci.* **2001**, *14*, 61–78.
19. Micallef, A.; Foglini, F.; Le Bas, T.; Angeletti, L.; Maselli, V.; Pasuto, A.; Taviani, M. The Submerged Paleolandscape of the Maltese Islands: Morphology, Evolution and Relation to Quaternary Environmental Change. *Mar. Geol.* **2013**, *335*, 129–147. [CrossRef]
20. Masson-Delmotte, V.; Zhai, P.; Pirani, A.; Connors, S.L.; Péan, C.; Berger, S.; Caud, N.; Chen, Y.; Goldfarb, L.; Gomis, M.I. (Eds.) *IPCC Climate Change 2021: The Physical Science Basis. Contribution of Working Group I to the Sixth Assessment Report of the Intergovernmental Panel on Climate Change*; Cambridge University Press: Cambridge, UK; New York, NY, USA, 2021; p. 2391. [CrossRef]

21. Valero-Garcés, B.; Morellón, M.; Moreno, A.; Corella, J.P.; Martín-Puertas, C.; Barreiro, F.; Pérez, A.; Giralt, S.; Mata-Campo, M.P. Lacustrine Carbonates of Iberian Karst Lakes: Sources, Processes and Depositional Environments. *Sediment. Geol.* **2014**, *299*, 1–29. [CrossRef]
22. Bonacci, O. Ground Water Behaviour in Karst: Example of the Ombla Spring (Croatia). *J. Hydrol.* **1995**, *165*, 113–134. [CrossRef]
23. Bonacci, O. *Karst Hydrology*; Springer: Berlin/Heidelberg, Germany, 1987; Volume 2, ISBN 978-3-642-83167-6.
24. Fleury, P.; Bakalowicz, M.; de Marsily, G. Submarine Springs and Coastal Karst Aquifers: A Review. *J. Hydrol.* **2007**, *339*, 79–92. [CrossRef]
25. White, W.B. Karst Hydrology: Recent Developments and Open Questions. *Eng. Geol.* **2002**, *65*, 85–105. [CrossRef]
26. van Hengstum, P.J.; Scott, D.B.; Gröcke, D.R.; Charette, M.A. Sea Level Controls Sedimentation and Environments in Coastal Caves and Sinkholes. *Mar. Geol.* **2011**, *286*, 35–50. [CrossRef]
27. Surić, M.; Juračić, M.; Horvatinčić, N.; Krajcar Bronić, I. Late Pleistocene-Holocene Sea-Level Rise and the Pattern of Coastal Karst Inundation: Records from Submerged Speleothems along the Eastern Adriatic Coast (Croatia). *Mar. Geol.* **2005**, *214*, 163–175. [CrossRef]
28. Bakalowicz, M. Karst and Karst Groundwater Resources in the Mediterranean. *Environ. Earth Sci.* **2015**, *74*, 5–14. [CrossRef]
29. Burnett, W.C.; Bokuniewicz, H.; Moore, W.S.; Taniguchi, M. Groundwater and pore water inputs to the coastal zone. *Biogeochemistry* **2003**, *62*, 3–33. [CrossRef]
30. Wirth, S.B.; Bouffard, D.; Zopfi, J. Lacustrine Groundwater Discharge Through Giant Pockmarks (Lake Neuchatel, Switzerland). *Front. Water* **2020**, *2*, 13. [CrossRef]
31. Schubert, M.; Scholten, J.; Schmidt, A.; Comanducci, J.F.; Pham, M.K.; Mallast, U.; Knoeller, K. Submarine Groundwater Discharge at a Single Spot Location: Evaluation of Different Detection Approaches. *Water* **2014**, *6*, 584–601. [CrossRef]
32. Benac, Č.; Juračić, M.; Matičec, D.; Ružić, I.; Pikelj, K. Fluviokarst and Classical Karst: Examples from the Dinarics (Krk Island, Northern Adriatic, Croatia). *Geomorphology* **2013**, *184*, 64–73. [CrossRef]
33. Donnaloia, M.; Giachetta, E.; Capolongo, D.; Pennetta, L. Evolution of Fluviokarst Canyons in Response to the Quaternary Tectonic Uplift of the Apulia Carbonate Platform (Southern Italy): Insights from Morphometric Analysis of Drainage Basins. *Geomorphology* **2019**, *336*, 18–30. [CrossRef]
34. Phillips, J.D. Historical Contingency in Fluviokarst Landscape Evolution. *Geomorphology* **2018**, *303*, 41–52. [CrossRef]
35. Silva, O.L.; Bezerra, F.H.R.; Maia, R.P.; Cazarin, C.L. Karst Landforms Revealed at Various Scales Using LiDAR and UAV in Semi-Arid Brazil: Consideration on Karstification Processes and Methodological Constraints. *Geomorphology* **2017**, *295*, 611–630. [CrossRef]
36. Gabriel, J.J.; Reinhardt, E.G.; van Hengstum, P.J.; Beddows, P.A.; Peros, M.C.; Davidson, D.E. Palaeoenvironmental Evolution of Cenote Aktun Ha (Carwash) on the Yucatan Peninsula, Mexico and Its Response to Holocene Sea-Level Rise. *J. Paleolimnol.* **2009**, *42*, 199–213. [CrossRef]
37. Kovacs, S.E.; van Hengstum, P.J.; Reinhardt, E.G.; Donnelly, J.P.; Albury, N.A. Late Holocene Sedimentation and Hydrologic Development in a Shallow Coastal Sinkhole on Great Abaco Island, The Bahamas. *Quat. Int.* **2013**, *317*, 118–132. [CrossRef]
38. Rowlands, G.; Purkis, S.; Bruckner, A. Diversity in the Geomorphology of Shallow-Water Carbonate Depositional Systems in the Saudi Arabian Red Sea. *Geomorphology* **2014**, *222*, 3–13. [CrossRef]
39. Paraschos, F.; Berke, M.A.; Koutsodendris, A.; Friedrich, O.; Sergiou, S.; Geraga, M.; Kaberi, H.; Williams, R.; Bailey, G.; Pross, J.; et al. The Holocene Evolution of a Sinkhole on the Southeast Red Sea Shelf: From Saline Palaeolake to Stratified Marine Setting. *Glob. Planet. Change* **2026**, *256*, 105176. [CrossRef]
40. Razum, I.; Miko, S.; Ilijanić, N.; Petrelli, M.; Röhl, U.; Hasan, O.; Giaccio, B. Holocene Tephra Record of Lake Veliko Jezero, Croatia: Implications for the Central Mediterranean Tephrostratigraphy and Sea Level Rise. *Boreas* **2020**, *49*, 653–673. [CrossRef]
41. Brunović, D.; Miko, S.; Ilijanić, N.; Peh, Z.; Hasan, O.; Kolar, T.; Šparica-Miko, M.; Razum, I. Holocene Foraminiferal and Geochemical Records in the Coastal Karst Dolines of Cres Island, Croatia. *Geol. Croat.* **2019**, *72*, 19–42. [CrossRef]
42. Balascio, N.L.; Zhang, Z.; Bradley, R.S.; Perren, B.; Dahl, S.O.; Bakke, J. A Multi-Proxy Approach to Assessing Isolation Basin Stratigraphy from the Lofoten Islands, Norway. *Quat. Res.* **2011**, *75*, 288–300. [CrossRef]
43. Long, A.J.; Woodroffe, S.A.; Roberts, D.H.; Dawson, S. Isolation Basins, Sea-Level Changes and the Holocene History of the Greenland Ice Sheet. *Quat. Sci. Rev.* **2011**, *30*, 3748–3768. [CrossRef]
44. Bakalowicz, M. Karst at Depth below the Sea Level around the Mediterranean Due to the Messinian Crisis of Salinity. Hydrogeological Consequences and Issues. *Geol. Belg.* **2014**, *17*, 96–101.
45. Ilijanić, N.; Brunović, D.; Miko, S.; Hajek Tadesse, V.; Hasan, O.; Razum, I.; Šparica Miko, M.; Mesić, S. Late Glacial and Holocene Paleoenvironmental Reconstruction of the Submerged Karst Basin Pirovac Bay on the Eastern Adriatic Coast. *J. Mar. Sci. Eng.* **2025**, *13*, 175. [CrossRef]
46. Korbar, T. Orogenic Evolution of the External Dinarides in the NE Adriatic Region: A Model Constrained by Tectonostratigraphy of Upper Cretaceous to Paleogene Carbonates. *Earth-Sci. Rev.* **2009**, *96*, 296–312. [CrossRef]

47. Pikelj, K.; Juračić, M. Eastern Adriatic Coast (EAC): Geomorphology and Coastal Vulnerability of a Karstic Coast. *J. Coast. Res.* **2013**, *289*, 944–957. [CrossRef]
48. Durn, G. Terra Rossa in the Mediterranean Region: Parent Materials, Composition and Origin. *Geol. Croat.* **2003**, *56*, 83–100. [CrossRef]
49. Babić, L.; Zupanič, J.; Vidović, J.; Razum, I.; Lužar-Oberiter, B.; Crnjaković, M. Preservation of Hanging Aeolian Deposits in Insular Karst Depressions: Sediment Sources and Implications for the Pleistocene Palaeogeography of the SE Adriatic Archipelago. *Aeolian Res.* **2013**, *11*, 171–189. [CrossRef]
50. Novak, A.; Šmuc, A.; Poglajen, S.; Vrabec, M. Linking the High-Resolution Acoustic and Sedimentary Facies of a Transgressed Late Quaternary Alluvial Plain (Gulf of Trieste, Northern Adriatic). *Mar. Geol.* **2020**, *419*, 106061. [CrossRef]
51. Ronchi, L.; Fontana, A.; Correggiari, A.; Asioli, A. Late Quaternary Incised and Infilled Landforms in the Shelf of the Northern Adriatic Sea (Italy). *Mar. Geol.* **2018**, *405*, 47–67. [CrossRef]
52. Ronchi, L.; Fontana, A.; Correggiari, A.; Remia, A. Anatomy of a Transgressive Tidal Inlet Reconstructed through High-Resolution Seismic Profiling. *Geomorphology* **2019**, *343*, 65–80. [CrossRef]
53. Amorosi, A.; Fontana, A.; Antonioli, F.; Primon, S.; Bondesan, A. Post-LGM Sedimentation and Holocene Shoreline Evolution in the NW Adriatic Coastal Area. *GeoActa* **2008**, *7*, 41–67.
54. Mamužić, P. *Osnovna Geološka Karta SFRJ, 1:100000, List Šibenik K33-8*; Institut za Geološka Istraživanja: Zagreb, Croatia; Savezni Geološki Zavod: Beograd, Serbia, 1971; p. 1.
55. Šparica, M.; Koch, G.; Belak, M.; Miko, S.; Šparica-Miko, M.; Viličić, D.; Dolenec, T.; Bergant, S.; Lojen, S.; Vreča, P.; et al. Recent Sediments of Makirina Cove (Northern Dalmatia, Croatia): Their Origin Viewed through a Multidisciplinary Approach. *Geol. Croat.* **2005**, *58*, 21–72. [CrossRef]
56. Miko, S.; Koch, G.; Mesić, S.; Šparica-Miko, M.; Šparica, M.; Čepelak, R.; Bačani, A.; Vreča, P.; Dolenec, T.; Bergant, S. Anthropogenic Influence on Trace Element Geochemistry of Healing Mud (Peloid) from Makirina Cove (Croatia). *Environ. Geol.* **2008**, *55*, 517–537. [CrossRef]
57. Bechor, B.; Sivan, D.; Miko, S.; Hasan, O.; Grisonic, M.; Rossi, I.R.; Lorentzen, B.; Artioli, G.; Ricci, G.; Ivelja, T.; et al. Salt Pans as a New Archaeological Sea-Level Proxy: A Test Case from Dalmatia, Croatia. *Quat. Sci. Rev.* **2020**, *250*, 106680. [CrossRef]
58. Mamužić, P. *Tumač OGK SFRJ 1:100000, List Šibenik K33-8*; Institut za Geološka Istraživanja: Zagreb, Croatia; Savezni Geološki Zavod: Beograd, Serbia, 1971.
59. Fritz, F. Postanak i Starost Vranskog Jezera Kod Biograda Na Moru. *Geol. Vijesn.* **1984**, *37*, 231–243.
60. Šikić, Z.; Pernar, N.; Yerkovich, B.B.; Rogošić, J.; Širac, S. Influence of Water Levels of Vrana Lake and the Adriatic Sea to the Water Chemistry of Vrana Lake. *Acta Adriat.* **2013**, *54*, 199–212.
61. Rubinić, J.; Katalinić, A. Régime Hydrologique Du Lac Vrana En Dalmatie (Croatie): Changements, Risques et Problèmes. *Hydrol. Sci. J.* **2014**, *59*, 1908–1924. [CrossRef]
62. Mitchum, R.M.; Vail, P.R.; Sangree, J.B. Seismic Stratigraphy and Global Changes of Sea Level, Part 6: Stratigraphic Interpretation of Seismic Reflection Patterns in Depositional Sequences. In *Seismic Stratigraphy—Applications to Hydrocarbon Exploration*; Payton, C.E., Ed.; American Association of Petroleum Geologists: Tulsa, OK, USA, 1977; pp. 117–134.
63. Blott, S.J.; Pye, K. Gradistat: A Grain Size Distribution and Statistics Package for the Analysis of Unconsolidated Sediments. *Earth Surf. Process. Landf.* **2001**, *26*, 1237–1248. [CrossRef]
64. Razum, I.; Ilijanić, N.; Petrelli, M.; Pawlowsky-Glahn, V.; Miko, S.; Moska, P.; Giaccio, B. Statistically Coherent Approach Involving Log-Ratio Transformation of Geochemical Data Enabled Tephra Correlations of Two Late Pleistocene Tephra from the Eastern Adriatic Shelf. *Quat. Geochronol.* **2023**, *74*, 101416. [CrossRef]
65. Heaton, T.J.; Köhler, P.; Butzin, M.; Bard, E.; Reimer, R.W.; Austin, W.E.N.; Bronk Ramsey, C.; Grootes, P.M.; Hughen, K.A.; Kromer, B.; et al. Marine20—The Marine Radiocarbon Age Calibration Curve (0–55,000 Cal BP). *Radiocarbon* **2020**, *62*, 779–820. [CrossRef]
66. Reimer, P.J.; Austin, W.E.N.; Bard, E.; Bayliss, A.; Blackwell, P.G.; Bronk Ramsey, C.; Butzin, M.; Cheng, H.; Edwards, R.L.; Friedrich, M.; et al. The IntCal20 Northern Hemisphere Radiocarbon Age Calibration Curve (0–55 Cal KBP). *Radiocarbon* **2020**, *62*, 725–757. [CrossRef]
67. Brunović, D.; Hasan, O.; Miko, S.; Georgiou, N.; Geraga, M.; Christodolou, D.; Dimas, X.; Ilijanić, N.; Papatheodorou, G. High-Resolution Seismic Record of the Quaternary Palaeoenvironments along a Dalmatian-Type Coast (Lošinj Channel, Adriatic Sea). *Mar. Geol.* **2024**, *474*, 107325. [CrossRef]
68. Mocochain, L.; Clauzon, G.; Bigot, J.Y.; Brunet, P. Geodynamic Evolution of the Peri-Mediterranean Karst during the Messinian and the Pliocene: Evidence from the Ardèche and Rhône Valley Systems Canyons, Southern France. *Sediment. Geol.* **2006**, *188–189*, 219–233. [CrossRef]
69. Lindhorst, K.; Vogel, H.; Krastel, S.; Wagner, B.; Hilgers, A.; Zander, A.; Schwenk, T.; Wessels, M.; Daut, G. Stratigraphic Analysis of Lake Level Fluctuations in Lake Ohrid: An Integration of High Resolution Hydro-Acoustic Data and Sediment Cores. *Biogeosciences* **2010**, *7*, 3531–3548. [CrossRef]

70. Bonacci, O.; Rubinić, J. Water Losses from a Reservoir Built in Karst: The Example of the Boljunčica Reservoir (Istria, Croatia). *Environ. Geol.* **2009**, *58*, 339–345. [CrossRef]
71. Gischler, E.; Schmitt, D.; Wiegand, A.; Behling, H.; Shumilovskikh, L.; Melles, M.; Wennrich, V.; Nolte, E.; Grego, J.; Anselmetti, F.S.; et al. Late Pleistocene to Holocene Sedimentation in the Great Blue Hole (Lighthouse Reef, Belize): Results from a 30 m Long Core. *Depos. Rec.* **2025**, *11*, 1376–1398. [CrossRef]
72. Shinn, E.; Reich, C.; Locker, S.; Hine, A. A Giant Sediment Trap in the Florida Keys. *J. Coast. Res.* **1996**, *12*, 953–959.
73. van Hengstum, P.J.; Maale, G.; Donnelly, J.P.; Albury, N.A.; Onac, B.P.; Sullivan, R.M.; Winkler, T.S.; Tamalavage, A.E.; MacDonald, D. Drought in the Northern Bahamas from 3300 to 2500 Years Ago. *Quat. Sci. Rev.* **2018**, *186*, 169–185. [CrossRef]
74. Ilijanić, N.; Miko, S.; Hasan, O.; Bakrač, K. Holocene Environmental Record from Lake Sediments in the Bokanjačko Blato Karst Polje (Dalmatia, Croatia). *Quat. Int.* **2018**, *494*, 66–79. [CrossRef]
75. Lambeck, K.; Antonioli, F.; Anzidei, M.; Ferranti, L.; Leoni, G.; Scicchitano, G.; Silenzi, S. Sea Level Change along the Italian Coast during the Holocene and Projections for the Future. *Quat. Int.* **2011**, *232*, 250–257. [CrossRef]
76. Trobec, A.; Šmuc, A.; Poglajen, S.; Vrabec, M. Submerged and Buried Pleistocene River Channels in the Gulf of Trieste (Northern Adriatic Sea): Geomorphic, Stratigraphic and Tectonic Inferences. *Geomorphology* **2017**, *286*, 110–120. [CrossRef]
77. Amorosi, A.; Maselli, V.; Trincardi, F. Onshore to Offshore Anatomy of a Late Quaternary Source-to-Sink System (Po Plain-Adriatic Sea, Italy). *Earth-Sci. Rev.* **2016**, *153*, 212–237. [CrossRef]
78. Furlani, S.; Cucchi, F.; Forti, F.; Rossi, A. Comparison between Coastal and Inland Karst Limestone Lowering Rates in the Northeastern Adriatic Region (Italy and Croatia). *Geomorphology* **2009**, *104*, 73–81. [CrossRef]
79. Wunsam, S.; Schmidt, R.; Müller, J. Holocene Lake Development of Two Dalmatian Lagoons (Malo and Veliko Jezero, Isle of Mljet) in Respect to Changes in Adriatic Sea Level and Climate. *Palaeogeogr. Palaeoclimatol. Palaeoecol.* **1999**, *146*, 251–281. [CrossRef]
80. Combourieu-Nebout, N.; Peyron, O.; Bout-Roumazeilles, V.; Goring, S.; Dormoy, I.; Joannin, S.; Sadori, L.; Siani, G.; Magny, M. Holocene Vegetation and Climate Changes in the Central Mediterranean Inferred from a High-Resolution Marine Pollen Record (Adriatic Sea). *Clim. Past* **2013**, *9*, 2023–2042. [CrossRef]
81. Siani, G.; Magny, M.; Paterne, M.; Debret, M.; Fontugne, M. Paleohydrology Reconstruction and Holocene Climate Variability in the South Adriatic Sea. *Clim. Past* **2013**, *9*, 499–515. [CrossRef]
82. Hajek-Tadesse, V.; Ilijanić, N.; Miko, S.; Hasan, O. Holocene Ostracoda (Crustacea) from the Shallow Lake Vrana (Dalmatia, Croatia) and Their Paleoenvironmental Significance. *Quat. Int.* **2018**, *494*, 80–91. [CrossRef]
83. Vacchi, M.; Marriner, N.; Morhange, C.; Spada, G.; Fontana, A.; Rovere, A. Multiproxy Assessment of Holocene Relative Sea-Level Changes in the Western Mediterranean: Sea-Level Variability and Improvements in the Definition of the Isostatic Signal. *Earth-Sci. Rev.* **2016**, *155*, 172–197. [CrossRef]
84. Farmer, D.M.; Freeland, H.J. The Physical Oceanography of Fjords. *Prog. Oceanogr.* **1983**, *12*, 147–220. [CrossRef]
85. Mejías, M.; Ballesteros, B.J.; Antón-Pacheco, C.; Domínguez, J.A.; Garcia-Orellana, J.; Garcia-Solsona, E.; Masqué, P. Methodological Study of Submarine Groundwater Discharge from a Karstic Aquifer in the Western Mediterranean Sea. *J. Hydrol.* **2012**, *464–465*, 27–40. [CrossRef]
86. Post, V.E.A.; Groen, J.; Kooi, H.; Person, M.; Ge, S.; Edmunds, W.M. Offshore Fresh Groundwater Reserves as a Global Phenomenon. *Nature* **2013**, *504*, 71–78. [CrossRef] [PubMed]
87. Bakken, T.H.; Ruden, F.; Mangset, L.E. Submarine Groundwater: A New Concept for the Supply of Drinking Water. *Water Resour. Manag.* **2012**, *26*, 1015–1026. [CrossRef]
88. Zuurbier, K.G.; Raat, K.J.; Paalman, M.; Oosterhof, A.T.; Stuyfzand, P.J. How Subsurface Water Technologies (SWT) Can Provide Robust, Effective, and Cost-Efficient Solutions for Freshwater Management in Coastal Zones. *Water Resour. Manag.* **2017**, *31*, 671–687. [CrossRef]

Disclaimer/Publisher's Note: The statements, opinions and data contained in all publications are solely those of the individual author(s) and contributor(s) and not of MDPI and/or the editor(s). MDPI and/or the editor(s) disclaim responsibility for any injury to people or property resulting from any ideas, methods, instructions or products referred to in the content.